Article

An Experimental Study of a Conventional Cylindrical Oscillating Water Column Wave Energy Converter: Fixed and Floating Devices

Wanan Sheng [1,*] and George Aggidis [2]

[1] Department of Aerospace and Mechanical Engineering, South East Technological University, R93 V960 Carlow, Ireland

[2] School of Engineering, Lancaster University, Lancaster LA1 4YW, UK; g.aggidis@lancaster.ac.uk

[*] Correspondence: wanan.sheng@setu.ie

Abstract: Oscillating water column (OWC) wave energy converters (WECs) are very popular types of wave energy converters due to their practical implementations, their versatility in deployment in different marine environments, and their high reliability in wave energy conversion. In development, different forms of OWCs have been proposed and advanced, such as fixed OWCs (on the shoreline, on breakwaters, or bottom standing) and floating OWCs (the spar and the backward-bent duct buoy, BBDB). In reality, a special type of OWC, the cylindrical OWC, is the simplest OWC in terms of its structural design and possible analytical/numerical solutions. However, such a simple OWC has not seen any practical applications because a cylindrical OWC is inefficient in wave energy absorption when compared to other types of OWC WECs. To study the simplest cylindric OWC, an experiment was carried out in a wave tank, and the relevant results are presented in this paper, with the aims of (i) analyzing the experimental data and exploring why such an OWC is inefficient in terms of wave energy absorption; (ii) providing experimental data for those who want experimental data to validate their numerical models; and (iii) establishing a baseline model so that comparisons can be made for improvements to the simple cylindrical OWC. As an example, an innovative solution was applied to the simple OWC such that its hydrodynamics and energy extraction performance can be significantly improved (the corresponding results will be presented in a separate paper).

Keywords: wave energy converter; oscillating water column; experimental study; cylindrical OWC; power performance

1. Introduction

Wave energy has much higher energy density when compared to other renewable resources, such as wind energy and solar energy. Thus, extracting wave energy from oceans is a very desirable addition to the energy mix in the future. This is especially true for countries that abound with wave energy resources [1]. However, wave energy production is very difficult since it involves large forces and very low velocity in the energy conversion process. Dealing with the large reciprocating forces and low reciprocating velocities in massive wave energy production is a challenging issue since this energy-converting process is the exact opposite of the conventional energy conversion process (i.e., electricity generation) in which a very large and steady rotational speed (generally 3000 RPM rotational speed, compared to the wave cycle at less than 10 RPM) and a low steady torque are applied for power conversion. In such a manner, the energy-converting system must sustain a continuous large reciprocating

force and address the inevitable issue of fatigue, which would inherently make wave energy converters very unreliable in energy production.

In fact, reliability-related issues in wave energy production are critical for all wave energy devices, and any successful wave energy devices must overcome these issues effectively. In the past decade, we have seen the failures of advanced wave energy technologies, such as the Pelamis and Oyster wave energy converters (WECs) [2,3], because of consistent issues concerning the devices' reliability. It should be noted that finding the root causes of these failures is not an easy process (see [4]), and some information is available on the website of Wave Energy Scotland (WES) [5].

Having been studied and developed for many years [6–9], and currently being an interesting topic in wave energy technologies [10–15], oscillating water column (OWC) wave energy converters (WECs) are well known to have the highest reliability in wave energy production (when compared to other wave energy technologies) due to their unique wave energy conversion processes. Their practical applications include the Land Installed Marine Power Energy Transmitter (LIMPET) in Scotland [16], a wave plant that generated wave energy power to the grid for more than 75,000 h in the period from 2001 to 2013. It was also reported that its energy availability achieved 98% in the last 4 years of operation [4]. Another example is the Mutriku wave energy plant, with OWCs built on breakwaters in Spain; the plant accumulated 2 GWh of energy from waves to the grid in 2020 [17]. A bottom-standing OWC plant, the Yongsoo plant in South Korea, is now used for generating hydrogen [18]. Another significant advancement is the OE buoy, a floating 'BBDB' (backward-bent duct buoy) OWC, developed in Ireland, and this BBDB OWC has finished its ¼-model sea trial in Galway Bay (Ireland), conducted for more than 4 years [19], and currently a full-scale, 35 m long device ('OE35') is being sea-trialled at the US Navy Wave Energy Test Site, WETS [20].

In addition to their high reliability for OWC WECs, their versatility in being deployed in different marine environments has attracted researchers and developers. OWCs can be designed as fixed-form devices, such as on the shoreline [16,21], on breakwaters [22,23], and in a bottom-standing form [18], or deployed as floating devices either in shallow waters or deep waters, such as BBDB OWC WECs [20,24], spar-type OWCs [25–27], etc.

In one aspect, OWC WECs would absorb wave power in a similar manner, with a large amplitude force and low velocity in the primary energy conversion stage. However, in another aspect, OWC WECs have a very different energy transmission process from other wave energy converters, in which energy transmission occurs in an indirect manner; that is, by applying air passage contraction in the air chamber, the very slow air flow (driven by waves) could be accelerated significantly, by 50–100 times, when the air flow reaches the air turbine. In summary, the energy transmission and conversion process in OWC WECs occurs in the following manner:

(1) The air flow near the water surface in the air chamber is initially driven by water body motion in the water column, and the corresponding air velocity is the same as the very slow velocity of the water body. This is the primary wave energy conversion.

(2) The air chamber is then contracted such that the air flow can be accelerated due to the fact that the flow continuity equation must be satisfied. The air flow would be accelerated by 50–100 times since the experimental results and numerical modelling have both shown that the area ratio of the orifice to the water surface area would ideally be about 1–2%.

(3) The much-accelerated, high-speed air flow can then drive an air turbine to rotate at a high rotational speed for energy conversion. The air turbine's rotational speed is generally in the range of 500–3000 RPM [28,29] compared to the wave cycle <10 RPM.

(4) With the high rotating speed of the air turbine, a low torque/force may be only needed for converting the required wave power in OWC WECs.

(5)   In a manner similar to the conventional energy conversion, with a high rotational speed and a low torque in OWC energy conversion, the OWC wave energy converters could generate wave power with a high reliability [8,9,30,31]. In this regard, OWCs are different from other wave energy converters.

It should be noted that the unique advantage for the OWC WEC is that in the OWC technologies, the speed acceleration of the air flow is through a soft transmission, that is, the air flow is accelerated simply through the contracted chamber, converting the energy due to the pressure in the air chamber into the high-speed air flow, in which no hard connection is required. This unique wave energy transmission process could make the OWC WECs most reliable among the wave energy technologies.

As desirable as other wave energy technologies, an OWC WEC must be efficient in extracting energy from waves, and this is the primary topic in both research and development for OWC technologies. Currently, researchers propose different ways for improving wave energy conversion efficiency by the OWC WECs. Examples include the U-OWC [23,32,33], which utilizes the interaction of the U channel and the water column for improving the OWC's energy absorption from waves. Included also are the dual- [12,34]/multi-chamber OWCs [35–38], in which the favorable interactions among the multi-chambers can be used for improving overall energy absorption from waves. For spar OWCs [25–27], they are designed to have two very different natural periods for the device heave motion and the internal water body motion, while examining the different shapes of BBDB OWCs [24,34,39–41] may improve the hydrodynamic performance of the BBDB OWCs for increasing their wave energy extraction.

To understand OWCs better, we can take the spar OWC as an example, since we have already seen the practical developments, such as the Marmok-A-5 in Spain [25] and the model in Portugal [26]. A question may be asked: Why do we need a long tube for a spar-OWC? Would a short tube be as efficient for the OWC?

To answer the question, we need to understand how the wave energy is extracted by the spar OWC. For the spar OWC, the main motion mode for wave energy conversion is the relative heave motion between the spar structure and the water body in the water column. To make such an OWC efficient, a large relative motion between these two heave motions in waves is very desirable. In design, the float of the spar OWC has a small mass and a small draft; thus, the spar structure has a small natural period in heave. In contrast, the long tube in the spar OWC means a long water body in the water column, thus a long natural period of the water body in the column; see [42,43]. So the spar OWC is so designed that a large difference between two natural periods of heave motions can be attained, and a large relative motion could be generated for the wave period between these two natural periods, since the two heave motions are in different phases under the wave excitation.

Having seen the special design for the spar OWCs, a major drawback for it is its large draft. For deploying such a floating structure, deep water is needed, and for such a large draft device, the installation/assembly, decommission and transportation will be also difficult. To reduce the draft, a sloped OWC is proposed (see details in [44]). However, there are no practical developments because such a solution may not benefit too much in solving the main problems for the spar OWCs.

A better solution would be the BBDB OWC, which can be regarded as bending the water column by 90° see the practical development by OceanEnergy Ltd. (Cork, Ireland) [20] and the developments in China [24,39]. In reality, BBDB OWCs have the advantage of a reduced draft; thus, the wave energy device can be fully assembled in harbors, and towed to the development site for deployment (decommissioning would be easily carried out by reversing the procedure). And the deployment of such an OWC device would be straightforward, by simple mooring and cable connections. A good example is the OceanEnergy OE35 plant (35 m long BBDB

device with a rated power of 1.0 MW). The wave power plant was manufactured and fully assembled in a shipyard in Portland (US), and then towed to Hawaii via the Columbia River and then across the East Pacific by a towboat in a journey of 43 days [45].

The BBDB OWC is generally efficient for extracting energy from waves, especially when the wave is in the right direction, and when the wave direction is not right, the wave energy extraction efficiency of the BBDB OWC would be reduced significantly. In addition, despite having been bent by 90° for the BBDB OWC, its draft can still be large if a large BBDB device is designed. For instance, the RM6 OWC has a draft of 17.5 m [46]. For manufacturing such a BBDB OWC device, a harbor of more than 17.5 m water depth is required, which may be generally beyond the existing harbors around the world.

This research aims to experimentally investigate a very simple OWC device, a cylindrical OWC with a small draft. From the experimental data, the simple OWCs are inefficient in terms of wave energy extraction. However, our focus for this experimental investigation is twofold: (1) to collect the experimental data for such a simple OWC so as to exploit why the cylindrical OWCs are so inefficient and to make experimental data available to the public for validating their numerical models, and (2) to make the simple cylindrical OWC as a baseline technology, to which any innovative solution (and hence improvements) applied to this simple OWC can be compared. In fact, an experimental study for improving the performance on the cylindrical OWC WEC is presented in a separate paper [47].

The remaining sections will be arranged as follows. In Section 2, the cylindrical OWC model in the experimental investigation is presented, and the relevant measurement systems and assessment methods are introduced in Section 3. In Section 4, the test results for the fixed cylindrical OWC are presented, while in Section 5, the test results for the floating cylindrical OWC are given. In Section 6, the comparisons are made for the fixed and floating OWCs, with a focus on their wave energy extraction capacities. Lastly, the conclusions are summarized in Section 7.

2. Wave Tank and Cylindrical OWC Model

2.1. Wave Tank

The model test was conducted in the ocean wave tank at Hydraulics and Maritime Research Centre (HMRC, Cork, Ireland), and the wave tank has dimensions of 25 m long, 18 m wide and 1 m deep (see Figure 1), the OWC model tested in a regular wave). A total of 40 flap-type wave makers installed in the tank are controlled independently for making waves of different types in the tank, such as regular waves, long-crested irregular waves, short-crested irregular waves, waves with an angle to the wave makers, focused waves, etc. In this OWC test, regular waves and long-crested irregular waves are used.
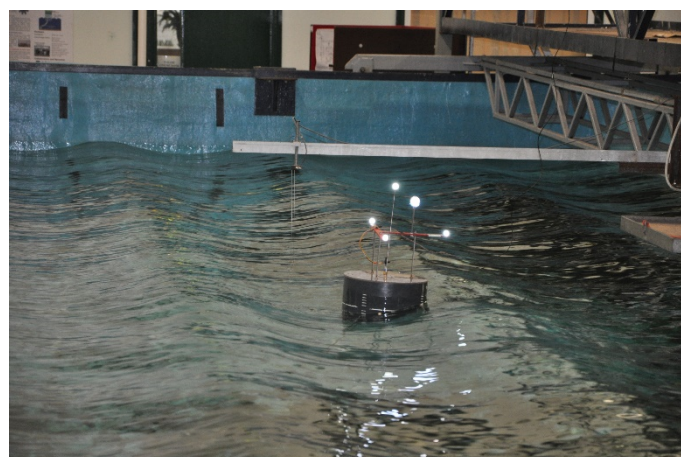

Figure 1. The cylindrical OWC tested in long-crested waves.

2.2. Cylindrical OWC Structure

The OWC wave energy converter for this experimental study is a simple cylindrical OWC, which was originally designed as a research OWC device [48]. The cylindrical OWC consists of a float of outer diameter 0.316 m, inner diameter 0.104 m (water column) and overall height 0.4 m. Both the fixed and floating OWCs have a draft of 0.3 m (the floating OWC has a weight of 20.98 kg). Figure 2 shows a fixed OWC in the wave tank, and Figure 3 is the floating OWC moored in the wave tank. Table 1 shows the relevant parameters of the testing model.
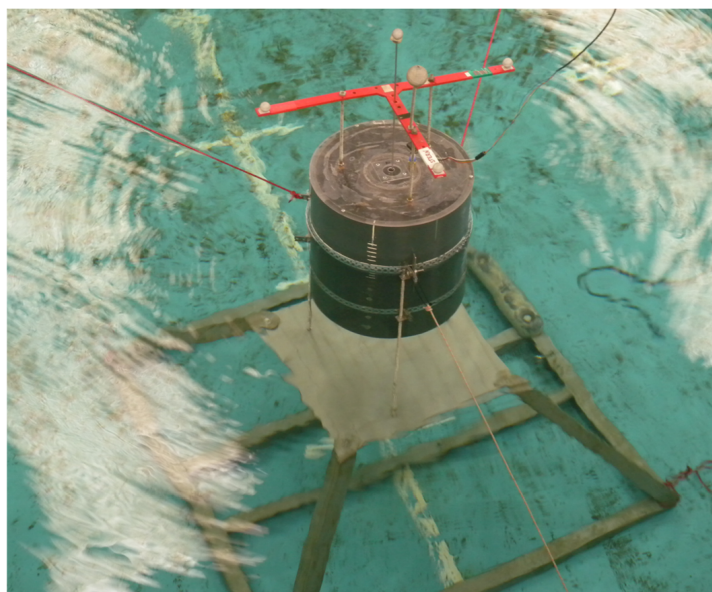

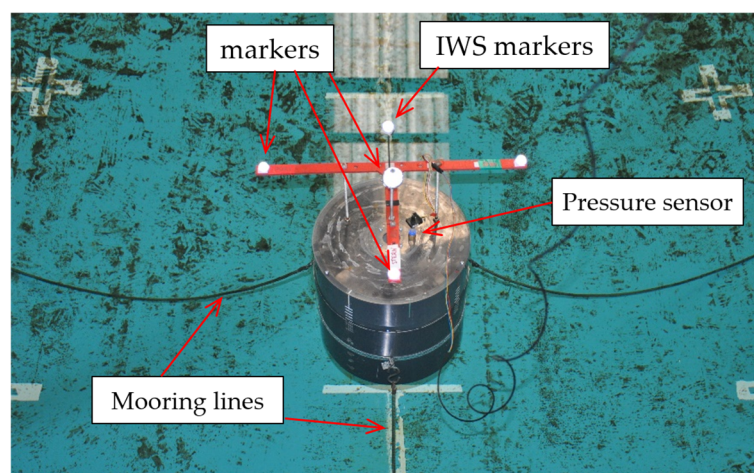**Figure 2.** The cylindrical OWC fixed on a frame in the wave tank (as a fixed cylindrical OWC).

Figure 3. The cylindrical OWC moored in the wave tank (a floating cylindrical OWC).

Table 1. Parameters for tank testing of the cylindrical OWC.

Parameter	Value
Outer diameter (m)	0.316
Inner diameter (m)	0.104
Draft (m)	0.300

Table 1. *Cont.*

Parameter	Value
Mass (kg)	20.98 (for floating device)
COG (m)	0.115 (from the bottom of the cylinder, for floating)
I_{xx} (kg $\times$ m^2)	0.65 (for floating)
I_{yy} (kg $\times$ m^2)	0.65 (for floating)
I_{zz} (kg $\times$ m^2)	0.25 (for floating)

2.3. Orifices (For Modelling Nonlinear Air Turbines)

In modelling a nonlinear air turbine PTO for the OWC WECs, such as the popular impulse air turbines [8], the nonlinear air turbines are simply modelled using orifices, and using orifices of different sizes for representing different damping relations between the pressure drop and the flow rate (as a reference, for a linear air turbine, it can be modelled in a similar way by applying larger orifices, but with the porous membrane (the carpet like texture) for damping the air flow through the orifices, such that the pressure drop and the flow rate can be roughly linear; see details in [49]).

To model a nonlinear air turbine, on the top of the air chamber, a Perspex plate (5 mm thick) with a large hole of 34.0 mm is fixed, and this large orifice represents an air passage with an area ratio 10.69% over the water column area. Obviously, such a large orifice would produce a very small damping to the air flow. To examine the different air damping levels by the orifices, five smaller orifices can be mounted over the large orifice for modelling larger damping levels to the air flow through the orifices. The diameters of the small orifices are given in Table 2, together with the corresponding area ratios over the sectional area of the water column.

Table 2. Orifice sizes and their ratios to the water column area (reduced by the rod of diameter 3 mm).

Orifice Diameter (mm)	Area Ratio to Area of the Water Column
8.0	0.51%
12.0	1.22%
14.0	1.70%
16.0	2.28%
22.0	4.36%

2.4. Data Acquisition Systems

2.4.1. Qualisys

Qualisys, a non-contact system of measuring the positions of the markers on the moving structures (the floating device in this case), consists of four cameras installed above the tank, and a T-Frame (and markers) is fixed on the floating body; see Figure 4.

To measure the motion of the internal water surface (IWS) related to the device, a small float (foam) is placed inside the water column, and it supports a small rod (3 mm in diameter) and a fluorescent ball on top of it; see Figure 5 for an illustration. The internal float is very light so it will follow the IWS motion accurately, as will the fluorescent ball for measuring the IWS motion.
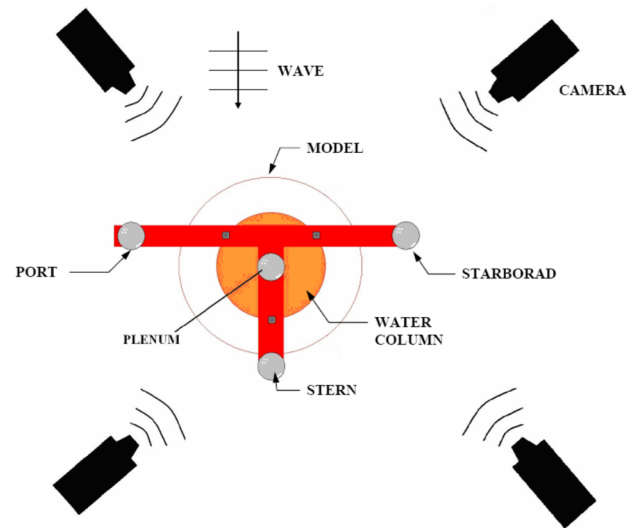
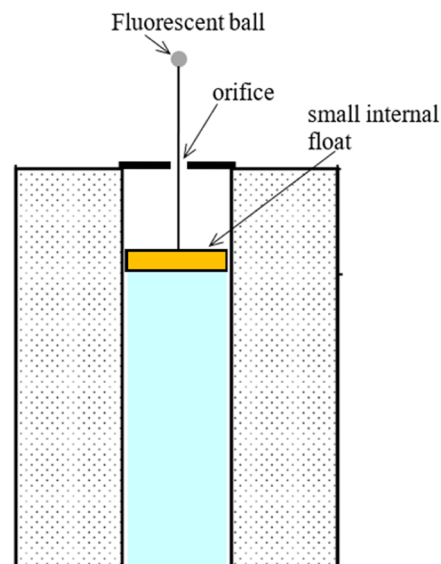**Figure 4.** Qualisys (camera system) and the model with the markers.

Figure 5. Measurement of the motion of the relative IWS.

2.4.2. LabVIEW System

In addition to the Qualisys system for measuring the motions of the structure and IWS, a LabVIEW system is applied for collecting all other measurements in the model test, such as the measurements of waves and the air chamber pressure.

The wave measurement is made via a wave probe which is placed 2 m away from the model in Figure 6. Such an arrangement would make the wave measurement not affected too much by the waves generated by the model (such as the scattered wave and the radiated wave).

A pressure sensor is installed on the top of the water column for measuring the air chamber pressure (see Figure 3). The measurement of the air chamber pressure is important for calculating power converted by the OWC, and such a measurement would be complementary to the measurement for the IWS motion, since both measurements can be used for calculating the absorbed power of the OWC, either independently or collectively. More details can be seen later in this paper.
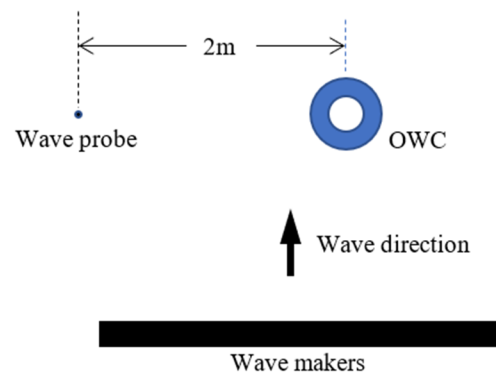
Figure 6. An illustration of the wave measurement in the model test in the wave tank.

2.4.3. Data Acquisition and Synchronisation

In the model test, two applied data acquisition systems (Qualisys and LabVIEW) are independent, but can be synchronized with a common trigger signal. The Qualisys has a built-in data acquisition system for recording the motions of the fluorescent balls mounted on the structure and a conversion software for converting the ball motions to the motions of the target structure. LabVIEW is a generalized data acquisition system for recording different signals via AD (analog–digital) conversion.

To synchronize the data acquisition, the LabVIEW system generates a trigger signal for the Qualisys system, such that the data acquisitions can be synchronized for both systems. However, this is the case if both systems were working well. It is found in the data postprocessing that the synchronization for two systems might not be working in some cases during the tank testing, that is, the aforementioned data acquisition systems were not synchronized.

In data postprocessing, it would be more difficult if two data acquisition systems were not synchronized. For instance, if the air chamber pressure (via LabVIEW) and the air flow through the orifice (via Qualisys) are not synchronized, the calculation of the extracted power by the OWC via both the measurements of air chamber pressure and the IWS motion would not work. In such a case, an option is to use the air chamber pressure to calculate the captured power. It should be noted that since the pressure and wave measurements are via the LabVIEW system, it is possible to align the wave measurement and the power conversion, while the extracted power calculation via the IWS only can be used to align the extracted power vs. the structural motions, but it is impossible to line it up with the wave measurement (see further details later).

3. Measurements and Data Processing

3.1. Qualisys and the Motion of the OWC Structure

The four cameras record the coordinates (motions) of each marker in a three-dimensional manner $(x,\ y,\ z)$. From these coordinates of the balls, it is possible to calculate the motions of the rigid body (6-DOF motions: surge, sway, heave, roll, pitch and yaw). The following principle is for converting Qualysis data into the structural motions.

The 3-D camera data are recorded during the wave testing, with a global system being defined in the Qualisys calibration in the tank. Suppose we have the coordinates of three markers (note: three markers are the minimum for deciding the structure motions), given by (x_1, y_1, z_1), (x_2, y_2, z_2) and (x_3, y_3, z_3), respectively.

For the floating rigid body, as a convention, 6-DOF motions can be used to describe the motion of the rigid body: three translational motions: surge (ξ), sway (η) and heave (ζ), and three rotational motions: roll (φ), pitch (θ) and yaw (ψ) [50].

The rotation matrix for each rotation is given as follows.

Matrix for rolling:

$$R_x = \begin{pmatrix} 1 & 0 & 0 \\ 0 & cos\varphi & -sin\varphi \\ 0 & sin\varphi & cos\varphi \end{pmatrix} \tag{1}$$

Matrix for pitching:

$$R_y = \begin{pmatrix} cos\theta & 0 & sin\theta \\ 0 & 1 & 0 \\ -sin\theta & 0 & cos\theta \end{pmatrix} \tag{2}$$

Matrix for yawing:

$$R_z = \begin{pmatrix} cos\psi & -sin\psi & 0 \\ sin\psi & cos\psi & 0 \\ 0 & 0 & 1 \end{pmatrix} \tag{3}$$

According to Diebel [50], there may be a total of 12 different ways to obtain the overall rotation matrix, depending on the order of the rotations. In Naval Architecture, three Euler angles (φ, θ, ψ) are mostly used to represent the rotation motions of the floating structures, i.e., rolling (around x-axis), pitching (around y-axis) and yawing (around z-axis). Following the convention, the order of the rotation is rolling first, then pitching and yawing last (Fossen and Smogeli 2004, [51]); therefore,

$$R = R_x R_y R_z = \begin{pmatrix} cos\theta cos\psi & sin\varphi sin\theta cos\psi - cos\varphi sin\psi & cos\varphi sin\theta cos\psi + sin\varphi sin\psi \\ cos\theta sin\psi & cos\varphi cos\psi + sin\varphi sin\theta sin\psi & cos\varphi sin\theta sin\psi - sin\varphi cos\psi \\ -sin\theta & sin\varphi cos\theta & cos\varphi cos\theta \end{pmatrix} \tag{4}$$

Corresponding to a point (x_1', y_1', z_1') on the rigid body, the point in the global coordinate system will be (x_1, y_1, z_1). The motion of the point can be represented by

$$\begin{pmatrix} x_1 \\ y_1 \\ z_1 \end{pmatrix} = R \begin{pmatrix} x_1' \\ y_1' \\ z_1' \end{pmatrix} + \begin{pmatrix} \xi \\ \zeta \\ \eta \end{pmatrix} \tag{5}$$

where ξ is surge, ζ sway and η heave.

To simplify the problem, we can assume the angular motions are small, that is, φ, θ, ψ are all small, so we have approximations:

$$\begin{cases} sin\varphi \approx \varphi;\ sin\theta \approx \theta;\ sin\psi \approx \psi \\ cos\,\varphi \approx cos\theta \approx cos\psi \approx 1 \end{cases} \tag{6}$$

By dropping the high-order terms, the total rotating matrix would be written as

$$R = \begin{pmatrix} 1 & -\psi & \theta \\ \psi & 1 & -\varphi \\ -\theta & \varphi & 1 \end{pmatrix} \tag{7}$$

Based on this simplified rotational matrix, it is possible to solve the structural motions: the translational motions, (ξ, ζ, η), and rotational motions, (φ, θ, ψ). The following are the methods for how to calculate the structural motions.

Consider another point on the structure, (x_2', y_2', z_2'), and its coordinate is (x_2, y_2, z_2) under the same translation and rotational motions, based on the relation

$$\begin{pmatrix} x_2 \\ y_2 \\ z_2 \end{pmatrix} = R \begin{pmatrix} x_2' \\ y_2' \\ z_2' \end{pmatrix} + \begin{pmatrix} \xi \\ \zeta \\ \eta \end{pmatrix} \tag{8}$$

Subtracting Equation (8) with Equation (5), we have

$$\begin{pmatrix} x_2 - x_1 \\ y_2 - y_1 \\ z_2 - z_1 \end{pmatrix} = \begin{pmatrix} 1 & -\psi & \theta \\ \psi & 1 & -\varphi \\ -\theta & \varphi & 1 \end{pmatrix} \begin{pmatrix} x_2' - x_1' \\ y_2' - y_1' \\ z_2' - z_1' \end{pmatrix} \tag{9}$$

This is a linear simultaneous equation, and can be used to solve the rotational angles, (φ, θ, ψ). In the tank test, the T-frame is such that a simplified calculation can be carried out. For instance, we can consider two points on the T-frame: the ball on the starboard side and the ball on the port side; thus, we could have $x_2' - x_1' = 0$ and $z_2' - z_1' = 0$, and using Equation (9), we have

$$\begin{cases} \psi = -\frac{x_2 - x_1}{y_2' - y_1'} \\ \varphi = \frac{z_2 - z_1}{y_2' - y_1'} \end{cases} \tag{10}$$

Using a similar method, we can obtain θ. Once we have all three rotational motions, we can easily calculate the translational motion by simply applying Equation (5):

$$\begin{pmatrix} \xi \\ \zeta \\ \eta \end{pmatrix} = \begin{pmatrix} x_1 \\ y_1 \\ z_1 \end{pmatrix} - R \begin{pmatrix} x_1' \\ y_1' \\ z_1' \end{pmatrix} \tag{11}$$

3.2. Motion of IWS

The measurement of the motion of the IWS can be used to calculate the flowrate through the orifice, since the air can be considered as incompressible in such a small model and the small pressure can be built up in the air chamber.

The IWS measurement is made by a float (a floating foam) on the IWS (see Figure 3) and the supported marker ("IWS marker"). The IWS marker can move relative to the T-frame. Hence, the relative motion of the IWS marker to the T-frame is actually the motion of the IWS in the water column.

Suppose the relative IWS motion is given as a time series, $x_7(t_i), (i = 1, \ldots, N)$, by a sampling time increment Δt (in the tank test, $\Delta t = \frac{1}{32}$ s), where N is the samples.

The velocity of the IWS can be calculated as (see [52]):

$$V_7(t_i) = \begin{cases} \frac{-3x_7(t_1) + 4x_7(t_2) - x_7(t_3)}{2\Delta t}, & for\ i = 1 \\ \frac{x_7(t_{i+1}) - x_7(t_{i-1})}{2\Delta t}, & for\ i = 2, \ldots, N-1 \\ \frac{x_7(t_{N-2}) - 4x_7(t_{N-1}) + 3x_7(t_N)}{2\Delta t}, & for\ i = N \end{cases} \tag{12}$$

Here, Equation (12) for velocity calculation has an accuracy of second order.

For the incompressible air, the flow rate is calculated as

$$Q(t_i) = V_7(t_i) A_0 \tag{13}$$

where A_0 is the sectional area of the water column at the water surface.

3.3. Flow Through Orifice

The flow rate through the orifice is the same as in Equation (13) due to the flow continuity for incompressible air. When the air flow is inhaled/exhaled through the orifice

of a sectional area A_1, with the reference flow velocity V_{70}, the flow rate through the orifice would be calculated as

$$Q = C_q V_{70} A_1 \qquad (14)$$

where C_q is the flow discharge coefficient, due to the non-uniform flow through the orifice. In our case, $C_q = 0.65$.

The relation between the wave-driven air velocity at IWS and the reference velocity of the air through the orifice is given as

$$V_{70} = \frac{1}{C_q} \frac{A_0}{A_1} V_7 \qquad (15)$$

3.4. Power Calculation

3.4.1. Power from the Measured Pressure and IWS Motions (P_1)

The power through the orifice is simply calculated in time series as

$$P_1(t) = p(t)Q(t) \qquad (16)$$

So the average power can be calculated as

$$\overline{P}_1 = \frac{1}{T} \int_0^T p(t)Q(t)dt \qquad (17)$$

where T is the wave period in regular waves, and the sampling time period in irregular waves.

For the sampled data, the average power is given by

$$\overline{P}_1 = \frac{1}{N} \sum_{i=1}^N p(t_i)Q(t_i) \qquad (18)$$

3.4.2. Power from the Chamber Pressure Only (P_2)

From the measured pressure, p, the reference velocity of air flow through the orifice can be calculated based on the Bernoulli's equation, as

$$V_{70} = \pm \sqrt{\frac{2|p|}{\rho_a}} \qquad (19)$$

where ρ_a is the air density.

The positive air flow velocity given in Equation (19) corresponds to positive air chamber pressure (exhalation), and a negative air chamber pressure corresponds to a negative velocity (inhalation). The corresponding flow rate through the orifice can be given by

$$Q = C_q V_{70} A_1 = sgn(p)\, C_q A_1 \sqrt{\frac{2|p|}{\rho_a}} \qquad (20)$$

where $sgn(p)$ indicates a negative sign when the chamber pressure is negative and a positive sign for a positive pressure. Using the flow discharge coefficient, $C_q = 0.65$, the relation between the flowrate and the chamber pressure can be seen as in Figure 7. Obviously, using the flow discharge coefficient $C_q = 0.65$, the flowrate and the pressure have been well correlated.
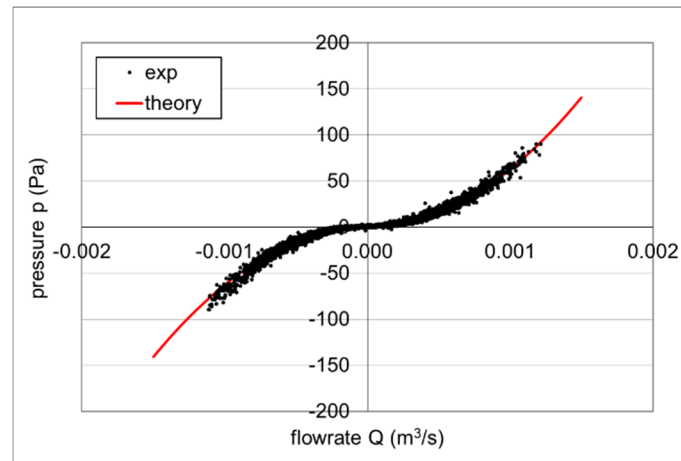
Figure 7. Experimental relation between the flowrate Q and the chamber pressure, *p*. Case: measurement vs. theory.

The power can be given as

$$P_2(t) = |p|C_q A_1 \sqrt{\frac{2|p|}{\rho_a}} = C_q A_1 \sqrt{\frac{2}{\rho_a}} |p(t)|^{\frac{3}{2}} \tag{21}$$

3.4.3. Power from the IWS Motions Only (P_3)

Based on the air flow velocity through the orifice, via Equation (15), applying Bernoulli's equation would lead to a pressure drop across the orifice:

$$p_3 = \frac{1}{2}\rho_a V_{70}^2 = \frac{\rho_a}{2C_q^2}\left(\frac{A_0}{A_1}\right)^2 V_7^2 \tag{22}$$

where p_3 is the pressure drop across the orifice, based on the reference velocity through the orifice, V_{70}.

The power is calculated:

$$P_3(t) = p_3(t)Q(t) = \frac{\rho_a A_0}{2C_q^2}\left(\frac{A_0}{A_1}\right)^2 |V_7(t)|^3 \tag{23}$$

The power is a function of the IWS velocity, V_7, which only depends on the IWS motion.

In theory, Equations (16), (21) and (23) should give the same powers if all measurements and the flow discharge coefficient are accurate. However, in practice, due to the errors in the measured data and in the flow discharge coefficient for different test conditions, slight differences can be seen when the power calculations are made by Equations (16), (21) and (23). Figures 8 and 9 show the comparisons for the calculated powers through the three different approaches for regular and irregular wave tests: 'P_1'— Equation (16) from both pressure and IWS measurement; 'P_2'—(21) from the pressure only; 'P_3'—Equation (23) from the IWS only. Generally, the three methods of power calculation are very close. However, it can be seen that the power calculated with the air pressure only is the smoothest, while the power calculations from the IWS only contain spikes. The reason for this is that the chamber pressure is less affected by the uneven events in the air chamber, while the IWS motion may be more affected by such uneven events.
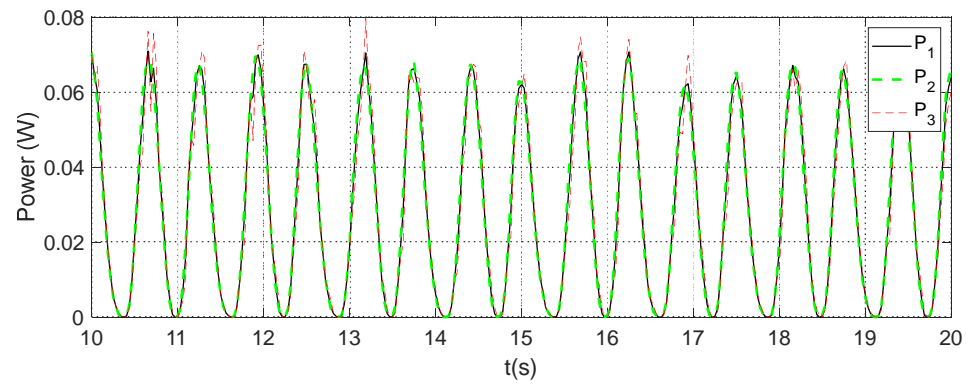
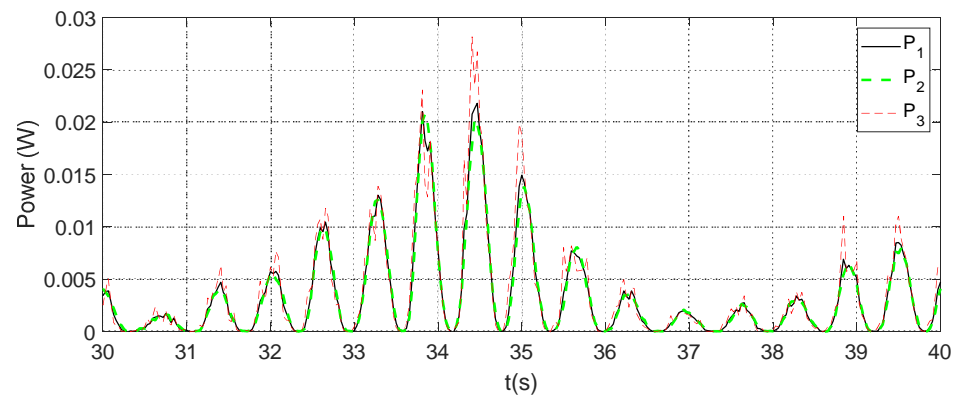**Figure 8.** Power comparison for three calculations in regular waves.

Figure 9. Power comparison for three calculations in irregular waves.

3.5. Capture Width and Efficiency

The average wave power per unit wave front length (a deep-water approximation is assumed for the simplicity of the wave power) is given by the following two equations.

For a regular wave:

$$E_{re} = \frac{\rho_w g^2}{32\pi} H^2 T \tag{24}$$

where H is the regular wave height, and T the wave period.

For an irregular wave:

$$E_{irr} = \frac{\rho_w g^2}{64\pi} H_s^2 T_e \tag{25}$$

where H_s is the significant wave height, and T_e the wave energy period.

So the wave energy capture width for a regular wave is

$$W = \overline{P}/E_{re} \tag{26}$$

For an irregular wave:

$$W = \overline{P}/E_{irr} \tag{27}$$

The efficiency of the wave energy capture is given by

$$\eta = \frac{W}{B} \times 100\% \tag{28}$$

where B is the overall width of the OWC buoy.

3.6. Responses (The Response Amplitude Operators, RAOs) in Regular Wave

Device motions:

$$H_i = \xi_i / H (i = 1, \dots, 6) \tag{29}$$

where H_i is the amplitude response operator (RAO) of the motions, i the index for the mode of motions, and ξ_i the height of the motion in waves.

Internal water surface (IWS), H_7:

$$H_7 = \xi_7 / H \tag{30}$$

where ξ_7 is the height of the IWS motion.

Pressure response, H_p:

$$H_p = p / H \tag{31}$$

where p is the height (from trough to peak) in the pressure signal.

Power capture response, H_P:

$$H_P = \frac{\overline{P}}{H^2} \tag{32}$$

where $\overline{P}$ is the average converted power of the OWC from waves.

4. Results and Analysis: Fixed Cylindrical OWC

The fixed cylindrical OWC in Figure 2 is supported using three small rods on a bottom-fixed frame, with a small plate being located at 0.3 m below the bottom of the OWC. Such an arrangement allows the fixed OWC to be isolated from the effects of other structures. Such an isolated OWC may be the simplest OWC structure, and its numerical modelling should be the easiest.

4.1. Regular Wave Tests

In wave tanks, regular wave tests are frequently used to examine the device performance of the marine structures in waves, generally given in the form of responses of the structure motions (and other responses too). For wave energy converters, the power capture response of a wave energy converter is a good indicator to show in what wave periods/frequencies the device can convert wave energy efficiently.

To obtain the full responses for the marine structure in waves, a series of regular waves must be used for testing. To achieve that, for a set of different chosen frequencies, the regular waves are generated ideally to have the same wave height. In our experimental investigation, 18 different frequencies/periods are used in the regular wave series test, and different wave heights (20 mm, 40 mm and 60 mm) may be used in the test for testing different series (the relevant experimental data are made available to the public in [53], where both regular and irregular wave tests for fixed and floating cylindrical OWCs can be downloaded for reference).

In principle, if the dynamic system is fully linear, then the responses (in the frequency domain) will be the same under the different wave heights. However, in the test of the simple OWC, since the orifices are used for the nonlinear PTO modelling in the OWC device, the corresponding dynamic systems are not linear. Therefore, the different wave heights can be used to examine the system's responses to different wave heights, that is, the nonlinearities in the dynamic system. Figure 10 show the responses of the IWS (motion) in different wave heights (H = 20 mm and H = 40 mm) for an orifice = 12 mm. Obviously, in the larger wave height, the orifice could produce a larger damping to the IWS motion, because the IWS responses for H = 40 mm have no obvious peak responses at the resonance period (T_0 = 1.25 s, see below) unlike the responses in the smaller waves, H = 20 mm. The

reason for this is that the IWS responses have more damping due to the orifice in a wave height of 40 mm compared to a wave height of 20 mm.
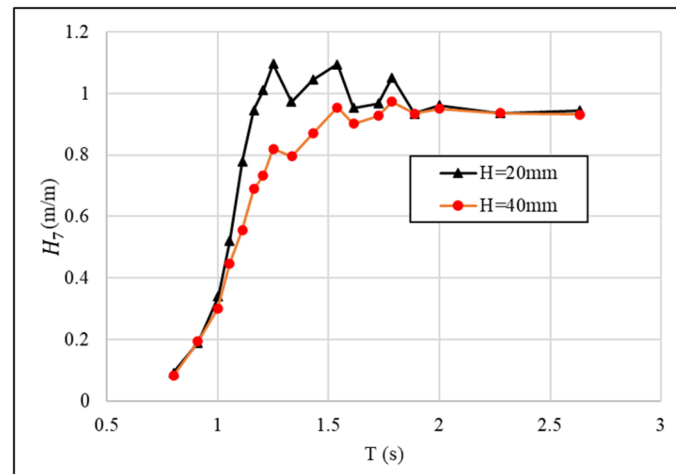

Figure 10. The responses of IWS under the different wave heights.

Motions of IWS

The IWS responses with different orifices can be seen in Figure 11 and the calculated natural periods of the IWS are also indicated. The natural period is calculated as T_0 = 1.177 s, following a semi-empirical formula, given in [43]:

$$T_0 = 2\pi\sqrt{\frac{D + 0.848R}{g}} \tag{33}$$

where D is the draft of the water column, and R is the radius of the water column.
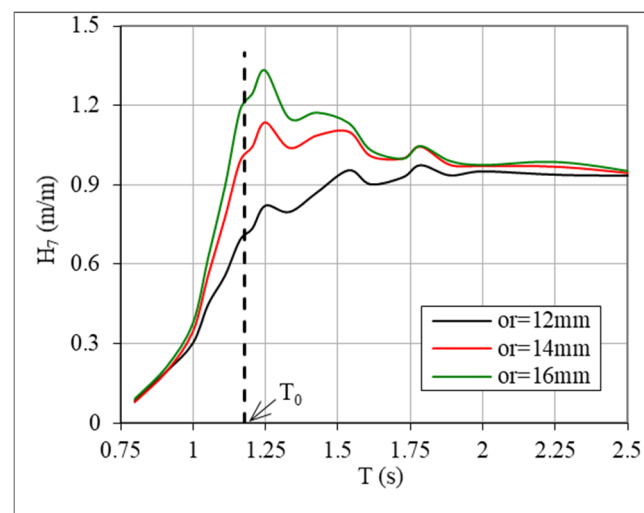
Figure 11. Responses of IWS for different orifices (wave height $\approx$ 40 mm).

For a comparison, the natural period of the IWS from the experimental data is about 1.25 s, indicated by the maximal IWS responses, specially for the case of an orifice diameter of 16 mm. It can be seen that there is some difference between the calculated natural period and the one from the experimental data, but they are quite close.

From the experimental results, it can be seen that the IWS responses are very dependent on the sizes of the orifices. This is understandable, because a smaller orifice means a larger

damping level to the IWS motions, and it is more evident for the IWS responses near the natural period.

It should be noted that for a nonlinear dynamic system, the response amplitude operators (RAOs) are given for reference, because of its wave amplitude dependence. This is different from the linear dynamic system, where the RAOs are independent of the wave amplitude. To make such an RAO more sensible, the wave heights in the regular wave tests are set to be the same or similar. For instance, for the case of H = 40 mm, the corresponding series tests should all have a wave height around H= 40 mm.

Figure 12 shows the comparison of the pressure responses with different sizes of orifices. Obviously, the smaller the orifice, the larger of the chamber pressure. This is evident at the larger wave periods, because the smaller orifices will create more damping to the air flow through the orifice; thus, a higher pressure can be built up in the air chamber.
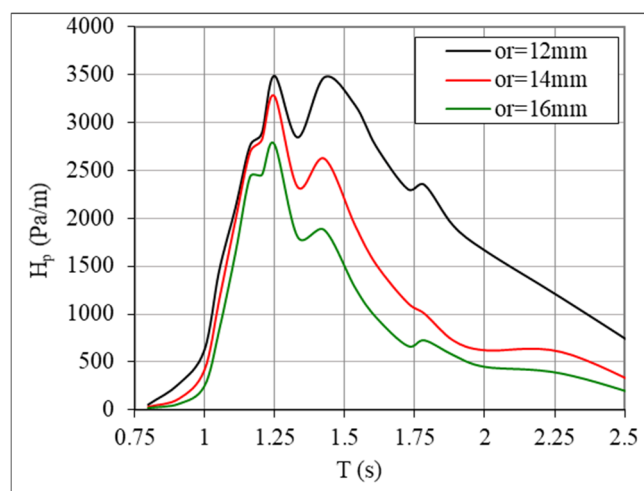

Figure 12. Responses of air chamber pressure for different orifices (wave height $\approx$ 40 mm).

Figure 13 shows the wave energy extraction responses of different orifices. For a smaller orifice, more extracted power is seen in the long waves, while with the larger orifices, more wave energy is extracted in the waves of small periods.
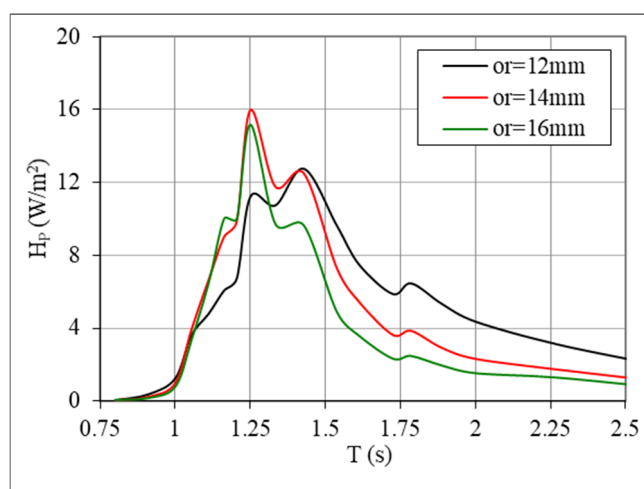

Figure 13. Responses of wave power extraction for different orifices (normalized by the wave height squared) (case: wave height $\approx$ 40 mm).

The wave energy extraction efficiency is seen in Figure 14 For such a simple fixed cylindrical OWC, the maximal energy conversion efficiency is about 4.2%. Indeed, this

cylindrical OWC has a very low energy efficiency in absorbing energy from waves. After all, this is a simple cylindrical OWC designed for a research project, simply aiming to understand OWC conversion of wave energy and to validate the established numerical model for the OWC; see [48,54]. For this experimental investigation, the relevant experimental data can be downloaded from the reference [53].
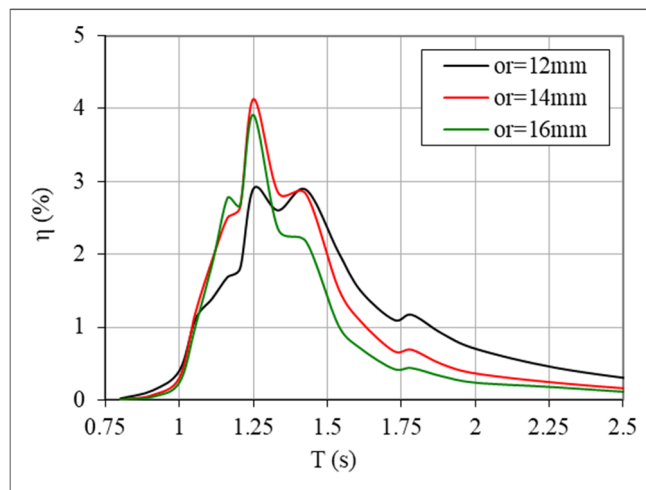

Figure 14. Efficiency of the wave energy extraction with the fixed OWC (wave height ≈ 40 mm).

4.2. Irregular Wave Test: Long-Crested Waves

Real ocean waves are random waves, that is, each wave cycle of the ocean wave would have different wave height and wave frequency (period) (see the recorded irregular wave in the wave tank in Figure 15). The irregular wave generated in the wave tank generally lasts for more than 4 min, allowing for a total 8192 sampling points at a sampling frequency of 32 Hz. Such series could guarantee more than 100 wave cycles in the record, even for the longest waves in this study, and it could ensure that the relevant statistical values from the irregular wave test would be meaningful.
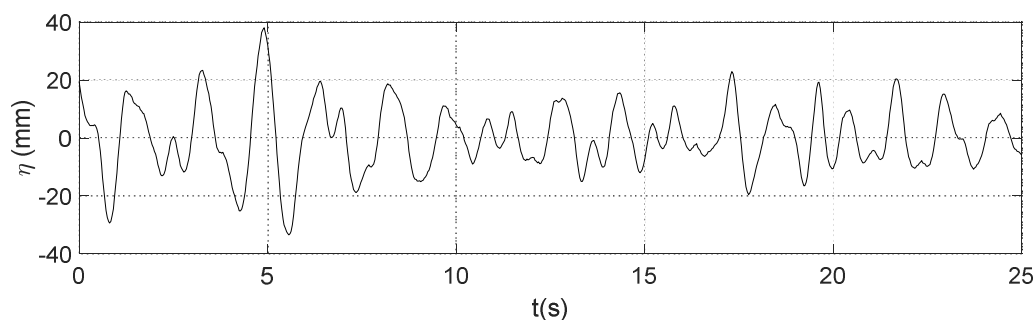

Figure 15. Irregular wave (long-crested) generated for the test.

The irregular wave test is used for examining the real performances of the marine structure in real ocean waves. To achieve that, the random irregular wave has been generated in the wave tank based on the wave statistical parameters, such as the significant wave height (H_s), wave spectral peak frequency (T_p) and spectrum type (Bretschneider or JONSWAP). Figure 16 shows a comparison of the target wave spectrum and the generated wave spectrum; the generated wave spectrum is very close to the target wave spectrum.

Table 3 lists the wave energy extraction efficiencies in different waves. From the table, it can be seen that the fixed OWC extracts most wave energy from the period $T_e = 1.08$ s. Also, with the orifice $\Phi = 12$ mm, the wave energy extraction is better than the case with the orifice $\Phi = 14$ mm.
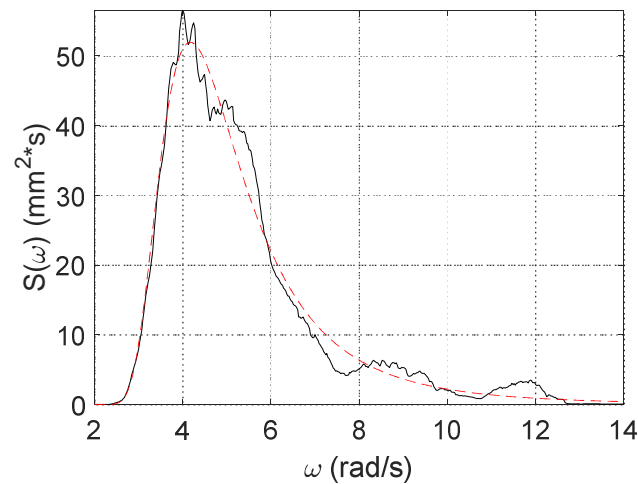
Figure 16. The spectrum of long-crested (2D) wave generated in the tank ('black line'), compared to the theoretical spectrum (Bretschneider, H_s = 49.20 mm, T_p = 1.507 s, 'red dashed line').

Table 3. Power extractions for different orifices.

T_e (s)	Energy Extraction Efficiency (%)		The Change for Φ = 14 mm (Compared to Φ = 12 mm)
	Φ = 12 mm	Φ = 14 mm	
0.89	0.867	0.770	−11.3%
1.08	3.690	2.526	−31.5%
1.30	2.826	1.804	−36.2%
1.70	1.104	0.809	−26.8%

5. Results and Analysis: Floating Cylindrical OWC (Original Form)

5.1. Mooring Setting

For the floating cylindrical OWC tests, three catenary mooring lines are used to moor the device in the wave tank. The mooring lines are evenly distributed 120° apart; see Figure 17 Each mooring line has a length of 4.0 m, the unit weight of the mooring line in water is 0.896 N/m, and the diameter of the mooring is 8 mm. The hanging points and the anchor points can be seen in Table 4.
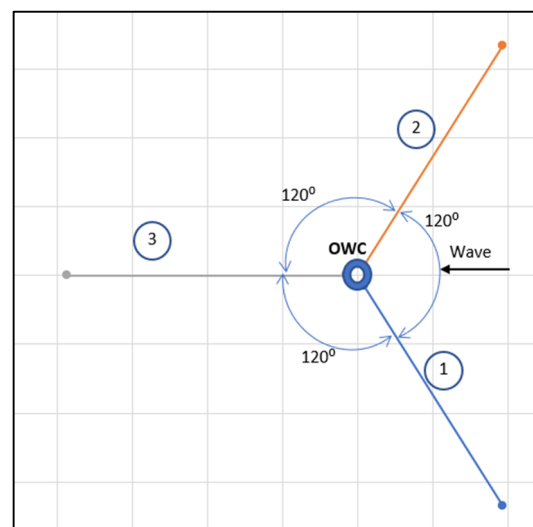

Figure 17. Catenary mooring line arrangement.

Table 4. Mooring connection points.

Mooring Line	Index	Hanging Point (m)	Anchor Point (m)
	x	0.084	1.934
Line 1	y	−0.145	−3.350
	z	−0.150	−1.000
	x	0.084	1.934
Line 2	y	0.145	3.350
	z	−0.150	−1.000
	x	−0.158	−3.868
Line 3	y	0.000	0.000
	z	−0.150	−1.000

5.2. Decay Test

Table 5 lists the natural periods of the motions for the floating OWC moored in the tank under the catenary mooring connection. From the table, due to the asymmetry in the surge and sway, their natural periods are very close, and for the same reason, the natural periods of roll and pitch motion are almost identical.

Table 5. Natural periods of the motions with moorings.

Motion Mode	Surge	Sway	Heave	Roll	Pitch	Yaw
Natural frequency in rad/s	0.485	0.503	4.928	3.642	3.653	1.280
Natural period in second	12.950	12.500	1.275	1.725	1.720	4.910

For the floating cylindrical OWC, it extracts wave energy mainly via the relative motion between the heave motions of the water body in the water column and the heave motion of the structure, while other motion modes could contribute little or nothing to the wave energy extraction for the OWC in terms of overall energy absorption. From the experimental results, we can see that the heave natural periods of the structure and the water body in the water column are very close, at 1.275 s (structure) vs. 1.250 s (water body), respectively. Such a small difference between these two natural periods means both the water body in the water column and the structure will move generally in phase, except the wave period is between these two natural periods of the heave motions (between 1.250 s and 1.275 s). Hence, the simple OWC would be very narrowly banded and thus very inefficient in terms of converting wave energy.

5.3. Regular Wave Tests

In a similar manner, the regular wave tests of the floating OWC include different orifices and different wave heights, such as H = 20 mm, 40 mm and 60 mm. For a sensible comparison, the responses presented in this section are for the regular waves with the wave height set at 40 mm as the target wave height.

Figure 18a shows the response of surge motions of the moored floating OWC structure. It can be seen that the response increases with the wave period. It should be noted that the responses in this figure are for the first-order responses, with the second-order responses excluded (the same for other motion modes). From the figure, we can see that the surge responses are independent of the orifice sizes.
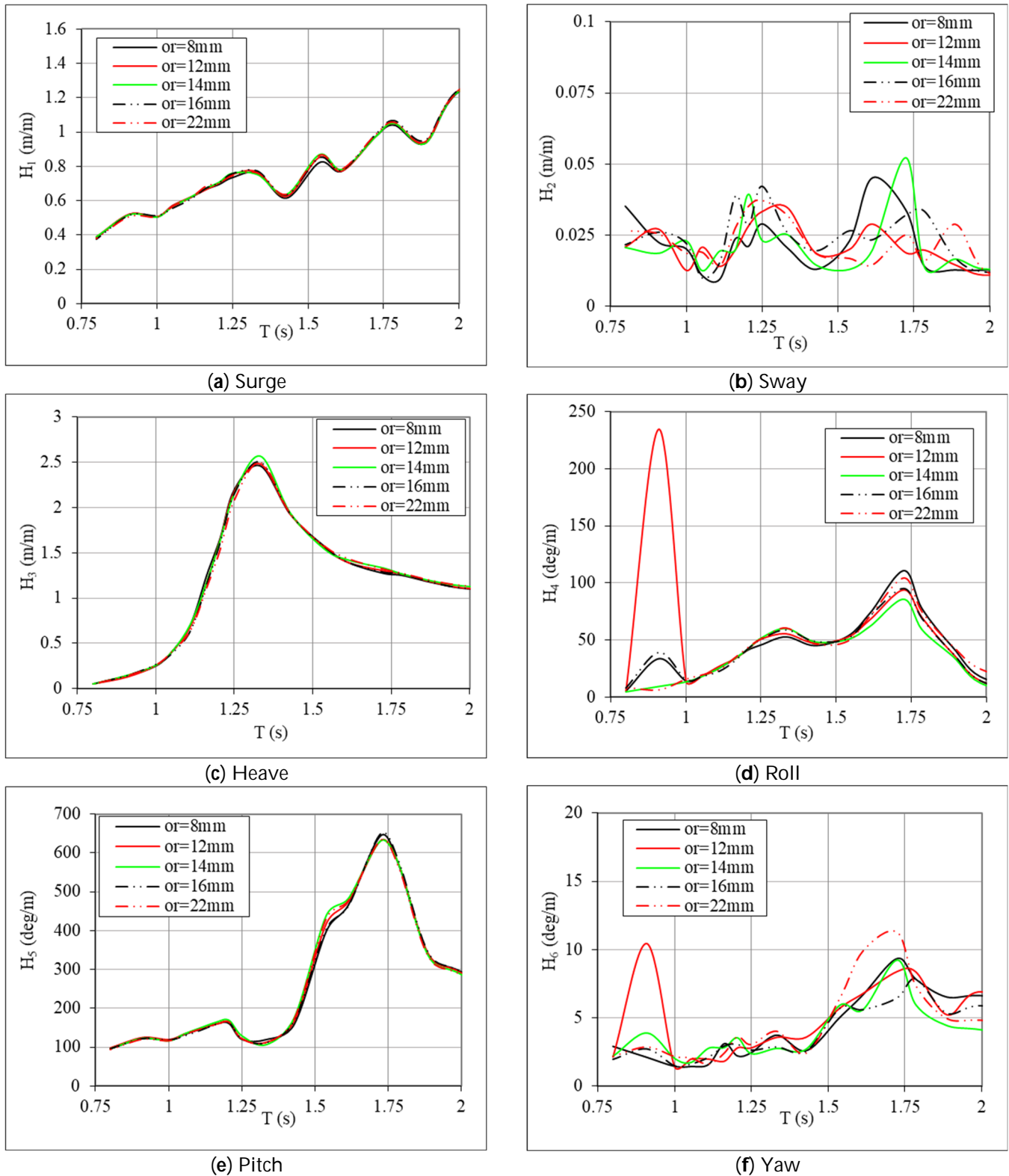
(**a**) Surge

(**b**) Sway

(**c**) Heave

(**d**) Roll

(**e**) Pitch

(**f**) Yaw

Figure 18. Motion responses of the structure in regular waves.

Figure 18b shows the response of sway motions. Obviously, the sway motion is very small (compare to the scale in Figure 18a). The responses are quite mixed under the different orifices, probably in the range of the experimental errors, and they can be ignored in the analysis.

Figure 18c shows the response of heave motions with the different orifices. It can be seen that the orifices have very small effects on the heave responses for this specific OWC, and only very small differences can be discerned in the responses. From the figure, the heave responses reach their maxima at its natural period ($T_0 = 1.275$ s).

Figure 18d shows the response of roll motion with the different orifices, and generally, some small roll responses from the experimental data can be seen when compared to the pitch responses in Figure 18e. However, we can see the extraordinary response in a certain period, and the analysis is given below.

In the regular wave tests, some extraordinary responses of roll motion can be seen in certain periods of waves. In fact, such a large amplitude response of rolling motion can be seen in other small devices, which is called instability of the rolling motion. It happens at the Mathieu resonance frequency [55] when the incoming wave frequency is close to twice the rolling resonance frequency, that is,

$$\omega_w = 2\omega_R \tag{34}$$

or in periods, as

$$T_w = \frac{1}{2}T_R \tag{35}$$

where ω_w (T_w) and ω_R(T_R) are the frequencies (periods) of incoming waves and the resonance of the roll.

From the experimental results, the extraordinary roll responses happen at the wave period $T = 0.91$ s, very close to half of the natural period of the roll motion ($T_R/2 = 1.725/2 = 0.863$ s).

From Figure 18d, it can also be seen that the instability of roll motion happens for the orifice of 12 mm only. But in reality, the instable roll does happen in other cases, mostly depending on the wave heights; the larger the wave height, the more evident the instable roll motion. In some cases, the instable roll motion is built up very quickly, and thus, it can be seen easily from the experimental data, while in some other cases, the instable roll motion is established in a very slow manner, so the instable motion has not been recorded due to the experimental time (normally 1 min for a regular wave test). This explains why, in Figure 18d, the instable roll responses may not be seen.

Figure 18e shows the response of pitch motions and it can be seen that the pitch responses are not very affected by the orifice sizes. The responses reach their maxima at the pitch natural period, $T_P = 1.72$ s.

Figure 18f shows the response of yaw motions, and these responses are very small when compared to pitch responses. It is understandable since, for such an axi-symmetrical OWC, there should be no yaw motion; however, in some cases, the yaw motions may be coupled with other motion modes, such as roll and pitch motions.

Figure 19 shows the IWS responses for different orifices, and the IWS response is obviously very dependent on the orifices; the larger the orifice, the larger the IWS responses.

Figure 20 shows the pressure responses under the different orifices: a larger orifice, a smaller pressure response, and Figure 21 shows the wave energy conversion efficiencies for different orifices. It can be seen from these two figures that the maximal pressure response and the maximal energy conversion efficiencies happen at the wave period $T = 1.25$ s.
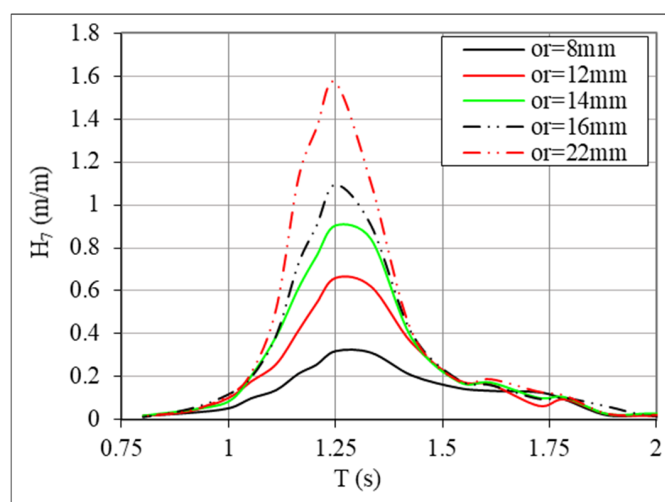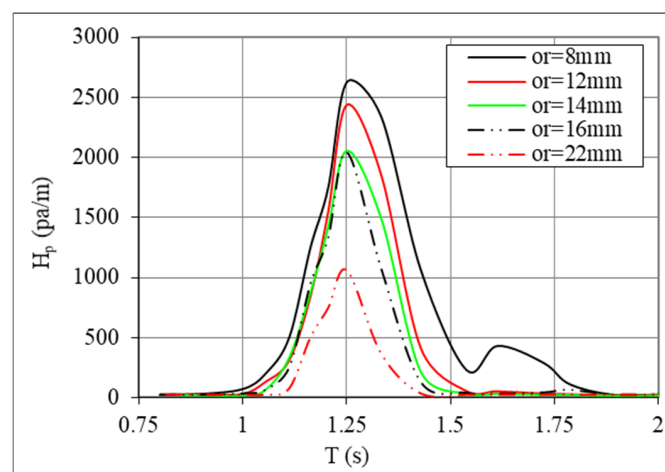
Figure 19. Responses of IWS motion (relative motion).

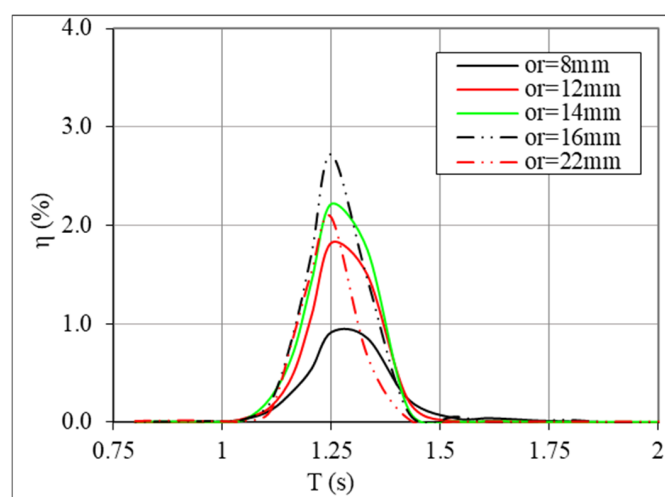**Figure 20.** Response of air chamber pressure.

Figure 21. Wave energy conversion efficiencies under different orifices.

5.4. Irregular Wave Test

Table 6 lists the wave energy extraction efficiencies of the floating cylindrical OWC from different wave states (long-crested wave). From the table, it can be seen that the floating OWC extracts the most wave energy from the period, T_e = 1.08 s.

Table 6. Wave energy extraction efficiencies of the floating OWC using different orifices in long-crested waves.

T_e (s)	Wave Energy Extraction Efficiency (%)		
	Φ = 12 mm	Φ = 14 mm	Φ = 16 mm
0.935	0.245	0.210	0.232
1.080	0.458	0.454	0.483
1.308	0.409	0.383	0.458
1.715	0.144	0.119	0.125

It can also be seen that, unlike the fixed OWC, the wave energy extractions are not so obvious for the small orifice, Φ = 12 mm. It looks like it is better than the case of Φ = 14 mm. However, the case with Φ = 16 mm is generally better than the case of Φ = 12 mm, except in the shortest waves in the list.

6. Comparisons Between the Fixed and Floating OWC

6.1. Responses

In this section, comparisons will be made for the responses for the fixed OWC and the floating OWC, for an orifice with a diameter Φ = 12 mm.

Figure 22 shows the IWS responses for the fixed OWC and the floating OWC. It can be seen that the IWS of the floating OWC is very narrowly banded, while the IWS in fixed OWC seems to have good responses in the long wave periods (they should be very close to unit, and the difference may be caused by the experimental errors).
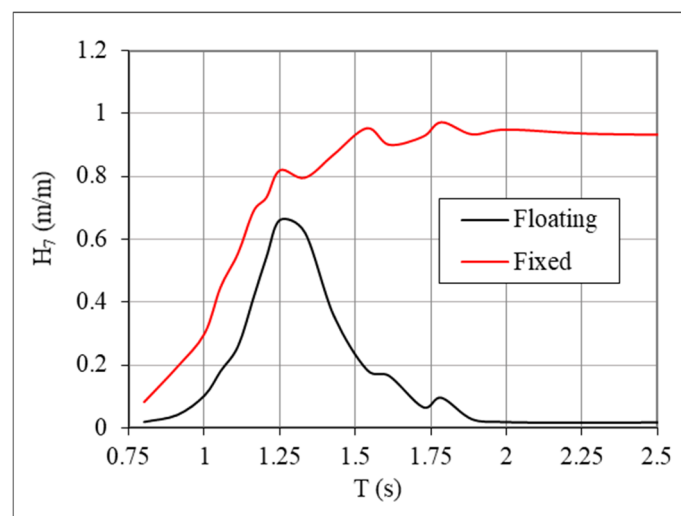

Figure 22. IWS responses.

Figure 23 shows the comparison of the responses of the air chamber pressure. It can be seen that for the fixed OWC, its pressure response has a much wider bandwidth and a much larger magnitude than for the floating OWC. For the floating OWC, the maximal pressure responses are at the wave period T = 1.25 s.

Figure 24 shows the response comparison of the wave energy extractions by the fixed and floating OWC, with Figure 25 showing the comparison of the efficiencies of wave energy conversion for the fixed and floating OWCs in regular waves. It can be seen again, in such a form, that the floating OWC is very inefficient and narrowly banded in terms of energy extractions from waves, even though the fixed OWC is much more efficient.
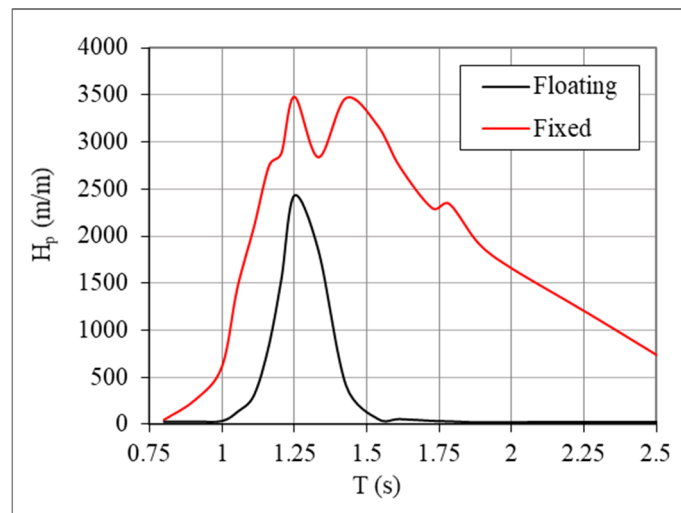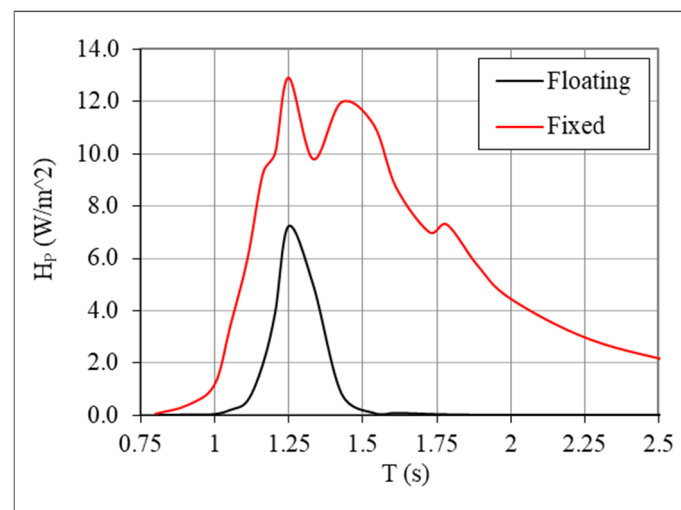
Figure 23. Air chamber pressure responses.

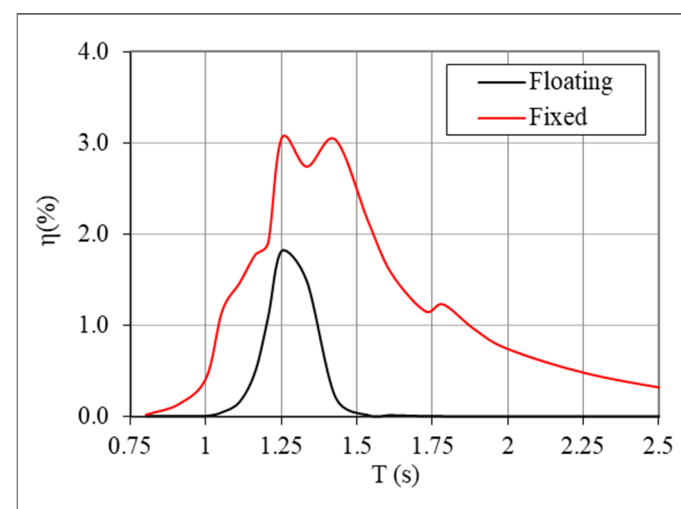**Figure 24.** Power extraction responses.

Figure 25. Efficiencies for fixed and floating OWCs.

6.2. Efficiencies of Wave Energy Conversion in Irregular Waves

Table 7 lists the wave energy extraction efficiencies in different wave states for both fixed and floating OWCs in irregular waves. From the table, it can be seen that the fixed OWC extracts wave energy generally many times when compared to the floating OWC, at 3.54 to 8 times, depending on the wave states.

Table 7. Power extractions for fixed and floating cylindrical OWC (Φ = 12 mm).

T_e (s)	Energy Extraction Efficiency (%)		Ratio (Fixed/Floating)
	Fixed	Floating	
0.89	0.867	0.245	3.54
1.08	3.690	0.458	8.06
1.30	2.826	0.409	6.91
1.70	1.104	0.144	7.67

7. Conclusions

This experimental investigation is the first part of the work on studying the cylindrical OWC WEC, with the hope of finding a solution for improving the performance of the cylindrical OWC. This part of the work aims to (i) investigate why the conventional cylindrical OWC is so inefficient in terms of wave energy extraction; (ii) provide the experimental data for the simple OWC in both fixed and floating forms for public use (data can be downloaded from [53]); and (iii) establish a baseline technology which provides the data for comparing any innovative solution to this simple OWC in terms of wave energy increment. A good solution has been presented in [47].

From the investigation, the following conclusions can be drawn:

(1) In the original simple form, the cylindrical OWC is inefficient in both fixed and floating forms. In the fixed form, the inefficiency is mostly due to the small water column (when compared to the overall size of the cylindrical OWC, 0.104 m vs. 0.316 m in diameter), while in the floating form, the structural heave motion and the water body in the cylindrical OWC have very close natural periods, which means that the structure and the water body of this simple OWC would move in phase under the wave excitation; hence, no large relative motion can be generated for the two heave motions, so this is inefficient.

(2) For calculating the extracted power from waves, three different methods may be applied: (i) via the combination of the pressure and the flowrate; (ii) via the pressure only; (iii) via the flowrate only. The comparisons have shown consistency in the calculation if the air discharge coefficient is taken appropriately. In this case, C_q = 0.65 has been taken.

(3) For practical purposes, measuring the air chamber pressure is a good approach in experimental study, since the air chamber pressure is less affected by the uneven events in the water column, such as the sloshing motions of the water surface in the chamber.

(4) The responses of the pressure in the air chamber and the IWS are very dependent on the orifice sizes; the larger the orifice, the smaller the pressure response and the larger the IWS motion response.

(5) The motion responses of the floating structure are not affected by the orifice sizes. This means that different damping levels of the airflow have no significant effects on the motions for this specific OWC. The reason may be the relatively small water column (when compared to the overall size of the OWC).

(6) For the floating OWC, the instable roll motion may happen at the Mathieu resonance frequency ($\omega_w = 2\omega_R$), mainly depending on the test conditions, such as the orifice size and the wave height.

It should be noted that the original cylindrical OWC WEC is a simple OWC for a research project, which is not designed or optimized to have a high efficiency in wave energy absorption. Having shown the inefficiency of the original OWC, especially in the floating form, an innovative solution has been applied to the simple OWC for increasing its energy conversion capacity significantly (see details in [47]).

References

1. Clément, A.; McCullen, P.; Falcão, A.F.d.O.; Fiorentino, A.; Gardner, F.; Hammarlund, K.; Lemonis, G.; Lewis, T.; Nielsen, K.; Petroncini, S.; et al. Wave energy in Europe: Current status and perspectives. *Renew. Sustain. Energy Rev.* **2002**, *6*, 405–431. [CrossRef]
2. BBC. 2014. Available online: https://www.bbc.com/news/uk-scotland-scotland-business-30151276 (accessed on 1 August 2024).
3. BBC. Aquamarine Power Calls in Administrators. 2015. Available online: https://www.bbc.com/news/uk-scotland-scotland-business-34659324 (accessed on 1 August 2024).
4. EC. *Study on Lessons for Ocean Energy Development (Final Report)*; Publications Office of the European Union: Luxembourg, 2017. [CrossRef]
5. WES. Knowledge Capture. Available online: https://library.waveenergyscotland.co.uk/knowledge-capture/ (accessed on 10 July 2024).
6. Evans, D.V. The oscillating water column wave-energy device. *IMA J. Appl. Math.* **1978**, *22*, 423–433. [CrossRef]
7. Evans, D.V.; Porter, R. Hydrodynamic characteristics of an oscillating water column device. *Appl. Ocean Res.* **1995**, *17*, 155–164. [CrossRef]
8. Falcao, A.; Henriques, J.C.C. Oscillating water column wave energy converters and air turbines: A review. *Renew. Energy* **2016**, *85*, 1391–1424. [CrossRef]
9. Rosati, M.; Henriques, J.C.C.; Ringwood, J.V. Oscillating-water-column wave energy converters: A critical review of numerical modelling and control. *Energy Convers. Manag. X* **2022**, *16*, 100322. [CrossRef]
10. Liu, Z.; Zhang, X.; Li, M. Experimental study on an OWC radial-flow impulse turbine in steady and reciprocating airflows. *Ocean Eng.* **2022**, *249*, 110876. [CrossRef]
11. Liu, Z.; Xu, C.; Kim, K.; Zhang, X.; Ning, D. Hydrodynamic and energy-harvesting performance of an isolated oscillating water column device: An experimental study. *Coast. Eng.* **2024**, *189*, 104459. [CrossRef]
12. Haghighi, A.T.; Nikseresht, A.H.; Hayati, M. Numerical analysis of hydrodynamic performance of a dual-chamber Oscillating Water Column. *Energy* **2021**, *221*, 119892. [CrossRef]
13. Zheng, S.; Zhang, Y.; Iglesias, G. Coast/breakwater-integrated OWC: A theoretical model. *Mar. Struct.* **2019**, *66*, 121–135. [CrossRef]
14. Konispoliatis, D.N. Floating Oscillating Water Column Wave Energy Converters: A Review of Developments. *J. Energy Power Technol.* **2024**, *6*, 2401005. [CrossRef]
15. Yang, S.; Zhu, W.; Tu, Y.; Cao, G.; Chen, X.; Du, Z.; Fan, J.; Huang, Y. Study on the influence of heave plate on energy capture performance of central pipe oscillating water column wave energy converter. *Energy* **2024**, *312*, 133517. [CrossRef]
16. Hydro, V. Voith Hydro. Available online: http://www.wavegen.co.uk/what_we_offer_limpet_islay.htm (accessed on 18 September 2011).
17. EVE. Mutriku OWC Plant. 2020. Available online: https://www.eve.eus/Jornadas-y-Noticias/Noticias/La-planta-de-energia-de-las-olas-de-Mutriku-bate?lang=en-gb (accessed on 9 December 2024).

18. OES. Wave Energy Developments Highlights. 2023. Available online: https://www.ocean-energy-systems.org/publications/oes-brochures/document/wave-energy-developments-highlights-2023/ (accessed on 25 June 2024).

19. Alcorn, R.; Healy, M.; Lewis, A.W. Lessons learned from the Galway bay Seatrials of the EU funded CORES project. In Proceedings of the 4 International Conference on Ocean Energy, Dublin, Ireland, 17–19 October 2012.

20. OceanEnergy. Ocean Energy: A World of Power. Available online: https://oceanenergy.ie/ (accessed on 25 June 2024).

21. WavEC. OWC PICO Wave Energy Plant. Available online: https://tethys.pnnl.gov/project-sites/pico-power-plant (accessed on 9 December 2024).

22. Mutriku. Mutriku Wave Energy Plant. Available online: https://www.power-technology.com/projects/mutriku-wave/ (accessed on 9 December 2024).

23. Arena, F.; Romolo, A. On design and building of a U-OWC wave energy converter in the Mediterranean sea: A case study. In Proceedings of the ASME 2013 32nd International Conference on Ocean, Offshore and Arctic Engineering, Nantes, France, 9–14 June 2013.

24. Wu, B.; Li, M.; Wu, R.; Chen, T.; Zhang, Y.; Ye, Y. BBDB wave energy conversion technology and perspective in China. *Ocean Eng.* **2018**, *169*, 281–291. [CrossRef]

25. Aldaiturriaga, E. Operating Experience of Marmok-A-5 OWC Wave Energy Converter at Bimep. 2018. Available online: https://www.ocean-energy-systems.org/publications/icoe/icoe-2018/document/operating-experience-of-marmok-a-5-owc-wave-energy-converter-at-bimep/ (accessed on 25 June 2024).

26. Portillo, J.C.C.; Collins, K.M.; Gomes, R.P.F.; Henriques, J.C.C.; Gato, L.M.C.; Howey, B.D.; Hann, M.R.; Greaves, D.M.; Falcao, A.F.O. Wave energy converter physical model design and testing: The case of floating oscillating-water-columns. *Appl. Energy* **2020**, *278*, 115638. [CrossRef]

27. Falcao, A.; Henriques, J.C.C.; Candido, J.J. Dynamic and optimization of the OWC spar buoy wave energy converter. *Renew. Energy* **2012**, *48*, 369–381. [CrossRef]

28. Setoguchi, T.; Takao, M. Current status of self rectifying air turbines for wave energy conversion. *Energy Convers. Manag.* **2006**, *47*, 2382–2396. [CrossRef]

29. Falcao, A.; Gato, L.M.C.; Henriques, J.C.C.; Borges, J.E.; Pereiras, B.; Castro, F. A novel twin-rotor radial-inflow air turbine for oscillating-water-column wave energy converters. *Energy* **2015**, *93*, 2116–2125. [CrossRef]

30. Lopez, I.; Pereiras, B.; Castro, F.; Iglesias, G. Holistic performance analysis and turbine-induced damping for an OWC wave energy converter. *Renew. Energy* **2016**, *85*, 1155–1163. [CrossRef]

31. Bull, D. An improved understanding of the natural resonances of moonpools contained within floating rigid-bodies: Theory and application to oscillating water column devices. *Ocean Eng.* **2015**, *108*, 799–812. [CrossRef]

32. Boccotti, P. Comparison between a U-OWC and a conventional OWC. *Ocean Eng.* **2007**, *34*, 799–805. [CrossRef]

33. Xu, C.; Liu, Z.; Tang, G. Experimental study of the hydrodynamic performance of a U-oscillating water column wave energy converter. *Ocean Eng.* **2022**, *265*, 112598. [CrossRef]

34. Chen, W.; Xie, W.; Zhang, Y.; Wang, C.; Wang, L.; Huang, L. Improving wave energy conversion performance of a floating BBDB-OWC system by using dual chambers and a novel enhancement plate. *Energy Convers. Manag.* **2024**, *307*, 118332. [CrossRef]

35. Zheng, S.; Antonini, A.; Zhang, Y.; Miles, J.; Greaves, D.M.; Zhu, G.; Iglesias, G. Hydrodynamic performance of a multi-Oscillating Water Column (OWC) platform. *Appl. Ocean Res.* **2020**, *99*, 102168. [CrossRef]

36. Mia, M.R.; Zhao, M.; Wu, H.; Palmer, H. Numerical simulation of a stationary offshore multi-chamber OWC wave energy. *Ocean Eng.* **2022**, *265*, 112546. [CrossRef]

37. Qian, K.; Chen, L.; Zhou, Y.; Ning, D. Hydrodynamics of an offshore multi-chamber OWC wave energy converter. *Energy* **2024**, *304*, 132239. [CrossRef]

38. Shalby, M.; Elhanafi, A.; Walker, P.; Dorrell, D.G. CFD modelling of a small–scale fixed multi–chamber OWC device. *Appl. Ocean Res.* **2019**, *88*, 37–47. [CrossRef]

39. Liu, Z.; Zhang, X.; Xu, C. Hydrodynamic and energy-harvesting performance of a BBDB-OWC device in irregular waves: An experimental study. *Appl. Energy* **2023**, *350*, 121737. [CrossRef]

40. Sheng, W. Motion and performance of BBDB OWC wave energy converters: I, hydrodynamics. *Renew. Energy* **2019**, *138*, 106–120. [CrossRef]

41. Sheng, W. Power performance of BBDB OWC wave energy converters. *Renew. Energy* **2019**, *132*, 709–722. [CrossRef]

42. Sarmento, A.J.N.A.; Falcao, A.F.D.O. Wave generation by an oscillating surface pressure and its application in wave-energy extraction. *J. Fluid Mech.* **1985**, *150*, 467–485. [CrossRef]

43. Sheng, W.; Alcorn, R.; Lewis, A. Assessment of primary wave energy conversions of oscillating water columns. I. Hydrodynamic analysis. *J. Renew. Sustain. Eng.* **2014**, *6*, 053113. [CrossRef]

44. CarbonTrust. Marine Energy Challenge: Oscillating Water Column Wave Energy Converter Evaluation Report. 2005. Available online: https://www.scribd.com/document/453737822/owc-report (accessed on 25 June 2024).

45. Bull, D.; Smith, C.; Jenne, D.S.; Jacob, P.; Copping, A.E.; Willits, S.; Fontaine, A.A.; Brefort, D.; Copeland, G.; FGordon, M.; et al. Reference Model 6 (RM6): Oscillating Wave Energy Converter, 2014; Sandia National Laboratory. Available online: https://tethys.pnnl.gov/publications/reference-model-6-rm6-oscillating-wave-energy-converter (accessed on 9 December 2024).

46. Sheng, W. An Experimental Study for Improving performance of a Cylindrical OWC WEC with a Heave Plate. *Renew. Sustain. Energy Rev.* 2025, *submitted*.

47. Sykes, R.K.; Lewis, A.W.; Thomas, G.P. Predicting hydrodynamic pressure in fixed and floating OWC using a piston model. In Proceedings of the 9th European Wave and Tidal Energy Conference, Southampton, UK, 5–9 September 2011.

48. Sheng, W.; Thiebaut, F.; Babuchon, M.; Brooks, J.; Alcorn, R.; Lewis, A. Investigation to air compressibility of oscillating water column wave energy converters. In Proceedings of the ASME 2013 32nd International Conference on Ocean, Offshore and Arctic Engineering, OMAE 2013, Nantes, France, 9–14 June 2012.

49. Sheng, W.; Aggidis, G. *Fundamentals of Wave Energy Conversions: The Dynamics of the Wave-Structure Interactions and Wave Energy Optimisation*; Eliva Press: Chișinău, Moldova, 2023.

50. Diebel, J. Representing attitude: Euler angles, unit quaternions, and rotation vectors. *Matrix* **2006**, *58*, 1–35.

51. Fossen, T.I.; Smogeli, O.N. Nonlinear time-domain strip theory formulation for low speed manoevering and station-keeping. *Model. Identif. Control* **2004**, *25*, 201–221. [CrossRef]

52. Yew, A. Numerical Differentiation: Finite Differences 2011. Available online: https://www.dam.brown.edu/people/alcyew/handouts/numdiff.pdf (accessed on 1 December 2024).

53. Sheng, W. *Experimental Data of a Cylindrical OWC Wave Energy Converter: Fixed and Floating OWCs [Data Set]*; Zenodo: Geneva, Switzerland, 2024. [CrossRef]

54. Sykes, R.K.; Lewis, A.W.; Thomas, G.P. A hydrodynamic study of a floating circular OWC. In Proceedings of the 8th European Wave and Tidal Energy Conference, Uppsala, Sweden, 7–10 September 2009; pp. 618–627.

55. Neves, M.A.S.; Rodriguez, C.A. On unstable ship motions resulting from strong non-linear coupling. *Ocean Eng.* **2006**, *33*, 1853–1883. [CrossRef]